Catalytic Cycle of a Divanadium Complex with Salen Ligands in O_2 Reduction: Two-Electron Redox Process of the Dinuclear Center (salen = *N,N′*-Ethylenebis(salicylideneamine))

Kimihisa Yamamoto, Kenichi Oyaizu, and Eishun Tsuchida*,†

Contribution from the Advanced Research Institute for Science & Engineering, Department of Polymer Chemistry, Waseda University, Tokyo 169-50, Japan

Received May 28, 1996[⊗]

Abstract: In an attempt to provide confirmation for the postulated mechanism of O_2 reduction in vanadium-mediated oxidative polymerization of diphenyl disulfide, a series of divanadium complexes containing salen ligand (salen = *N,N′*-ethylenebis(salicylideneamine)) were prepared, characterized, and subjected to reactivity studies toward dioxygen. A divanadium(III, IV) complex, [(salen)VOV(salen)][I_3] (**II**), was yielded both by treatments of solutions of [(salen)-VOV(salen)][BF_4]$_2$ (**I**) in acetonitrile with excess tetrabutylammonium iodide and by electroreduction of **I** followed by anion exchange with tetrabutylammonium triiodide. The complex **II** was characterized by a near-infrared absorption at 7.2×10^3 cm^{-1} ($\epsilon = 60.1$ M^{-1} cm^{-1} in acetonitrile) assigned to an intervalence transfer band. A crystallographically determined V(III)−V(IV) distance of 3.569(4) Å is consonant with the classification of **II** as a weakly coupled Type II mixed-valence vanadium ($\alpha = 3.0 \times 10^{-2}$). Oxidation of the cation [(salen)VOV(salen)]$^+$ with O_2 in dichloromethane yielded spontaneously the deep blue, mixed valent, divanadium(IV, V) species [(salen)VOVO-(salen)]$^+$ which was structurally characterized both as its triiodide (**III**) and perchlorate (**IV**) salts. Crystal data for **III**: triclinic space group $P\bar{1}$ (no. 2), $a = 14.973(2)$ Å, $b = 19.481(2)$ Å, $c = 14.168(2)$ Å, $\alpha = 107.00\ (1)°$, $\beta = 115.56(1)°$, $\gamma = 80.35(1)°$, $V = 3561.3(9)$ Å^3, $Z = 4$, $D_{calc} = 1.953$ g/cm^3, μ (MoKα) = 31.74 cm^{-1}, final $R = 0.057$ and $R_w = 0.065$. Crystal data for **IV**: triclinic space group $P\bar{1}$ (no. 2), $a = 11.923(3)$ Å, $b = 14.25(1)$ Å, $c = 11.368(7)$ Å, $\alpha = 112.92(5)°$, $\beta = 92.76(4)°$, $\gamma = 99.13(4)°$, $V = 1743(1)$ Å^3, $Z = 2$, $D_{calc} = 1.537$ g/cm^3, μ (CuKα) = 57.69 cm^{-1}, final $R = 0.042$ and $R_w = 0.061$. The complexes **III** and **IV** were deoxygenated in strongly acidic nonaqueous media to produce [(salen)VOV(salen)]$^{3+}$ as a high-valent complex whose reversible two-electron redox couple (VOV^{3+}/VOV^{+}) at 0.44V vs Ag/AgCl has been confirmed. Its ability to serve as a two-electron oxidant provided a unique model of a multielectron redox cycle in oxidative polymerization.

Introduction

The capacity of metalloenzymes to transduce energy *via* synergetic electron transfer (ET) for the assimilative reductions of small molecules such as carbon dioxide and dinitrogen and O_2-oxidations in dissimilatory processes[1] poses a considerable challenge to modeling the biological processes. As recent topics, the X-ray structures of cytochrome *c* oxidases which provoke four-electron reduction of O_2 to H_2O attract much attention[2] though the structures of the intermediate O_2 adducts or their catalytic mechanisms have not been realized yet. As to the four-electron reduction system of O_2, much effort has been spent to establish an effective electrocatalyst which operates near the thermodynamic potential.[3] Recent trends involve the use of multinuclear complexes having O_2 coordination sites. Anson and co-workers found that four-electron reduction of O_2 is accomplished at 0.30 V vs SCE by using a tetraruthenated cobalt tetrapyridylporphyrin, with continued diligence toward unraveling the mechanism.[4] Our interest is, on the other hand, directed toward the application of well-defined four-electron reduction systems of O_2 to molecular syntheses.[5] Indeed, a number of important biological and industrial processes involve metal-catalyzed oxidation of organic substrates, and, for this purpose, the use of dioxygen as the ultimate oxidant has obvious advantages in terms of cost and handling use.[6]

We have established the novel synthetic route of poly(*p*-phenylene sulfide), an important engineering plastic, by the oxovanadium-catalyzed O_2-oxidative polymerization of diphenyl disulfide.[7] Bis(acetylacetonato)oxovanadium(IV), VO(acac)$_2$, acts as an excellent catalyst in nonaqueous acidic media, but

† CREST investigator (1996−2000), JSTC.

⊗ Abstract published in *Advance ACS Abstracts,* December 1, 1996.

(1) (a) Brudvig, G. W.; Thorp, H. H.; Grabtree, R. H. *Acc. Chem. Res.* **1991**, *24*, 311. (b) *Biological Nitrogen Fixation*; Stacey, G., Burris, R. H., Evans, H. J., Eds.; Chapman & Hill: New York, 1992. (c) *Biology and Biochemistry of Nitrogen Fixation;* Dilworth, M. J., Glenn, A. R., Eds.; Elsevier: Amsterdam, 1991. (d) *Manganese Redox Enzymes;* Pecoraro, V. L., Ed.; VCH Publishers Inc.: New York, 1992.

(2) (a) Iwata, S.; Ostermeier, C.; Ludwig, B.; Michel, H. *Nature* **1995**, *376*, 660. (b) Tsukihara, T.; Aoyama, H.; Yamashita, E.; Tomizaki, T.; Yamaguchi, H.; Shinzawa-Itoh, K.; Nakashima, R.; Yaono, R.; Yoshikawa, S. *Science* **1995**, *269*, 1069.

(3) (a) Chang, C. K.; Liu, H. Y.; Abdalmuhdi, I. *J. Am. Chem. Soc.* **1984**, *106*, 2725. (b) Ni, C.-L.; Abdalmuhdi, I.; Chang, C. K.; Anson, F. C. *J. Phys. Chem.* **1987**, *91*, 1158. (c) Shi, C.; Anson, F. C. *J. Electroanal. Chem.* **1990**, *293*, 165. (d) Zhang, J.; Anson, F. C. *J. Electroanal. Chem.* **1992**, *341*, 323. (e) Shi, C.; Anson, F. C. *Inorg. Chem.* **1990**, *29*, 4298. (f) Collman, J. P.; Denisevich, P.; Konai, Y.; Marrocco, M.; Koval, C.; Anson, F. C. *J. Am. Chem. Soc.* **1980**, *102*, 6027. (g) Collman, J. P.; Kim, K. *J. Am. Chem. Soc.* **1986**, *108*, 7847.

(4) (a) Shi, C.; Anson, F. C. *J. Am. Chem. Soc.* **1991**, *113*, 9564. (b) Shi, C.; Anson, F. C. *Inorg. Chem.* **1995**, *34*, 4554. (c) Steiger, B.; Anson, F. C. *Inorg. Chem.* **1995**, *34*, 3355. (d) Steiger, B.; Anson, F. C. *Inorg. Chem.* **1994**, *33*, 5767. (e) Shi, C.; Anson, F. C. *Inorg. Chem.* **1992**, *31*, 5078. (f) Steiger, B.; Shi, C.; Anson, F. C. *Inorg. Chem.* **1993**, *32*, 2107.

(5) (a) Yamamoto, K.; Shouji, E.; Nishide, H.; Tsuchida, E. *J. Am. Chem. Soc.* **1993**, *115*, 5819. (b) Yamamoto, K.; Shouji, E.; Suzuki, F.; Kobayashi, S.; Tsuchida, E. *J. Org. Chem.* **1995**, *60*, 452. (c) Yamamoto, K.; Kobayashi, S.; Shouji, E.; Tsuchida, E. *J. Org. Chem.* **1996**, *61*, 1912.

(6) (a) Thiyagarajan, B.; Kerr, M. E.; Bruno, J. W. *Inorg. Chem.* **1995**, *34*, 3444. (b) *Dioxygen Activation and Homogeneous Catalytic Oxidation;* Simandi, L. I., Ed.; Elsevier: Amsterdam, 1991; Vol. 66. (c) Sheldon, R. A.; Kochi, J. M. *Metal-Catalyzed Oxidation of Organic Compounds;* Academic Press: New York, 1981.

S0002-7863(96)01779-9 CCC: $12.00

mechanistic analysis of the redox process involved in the catalytic cycle is made difficult because of the lability of the β-diketone ligand.[8] We previously described the electron transfer chemistry of a more stable model of the acetylacetonato catalyst, VO(salen) (salen = *N*,*N*′-ethylenebis(salicylideneamine)), which revealed that a μ-oxo divanadium(IV) complex ([(salen)VOV(salen)]$^{2+}$, VOV^{2+}) is formed in strongly acidic nonaqueous media.[9] The two-electron redox couple of the complex ($VOV^{3+} + 2e^- \rightleftarrows$ Ã VOV^+) has been defined in CH_3CN by electrochemical measurements.[9]

Since the oxidative polymerization of diphenyl disulfide catalyzed by $VO(acac)_2$ results in a selective formation of thioether bonds without any oxygenated compounds such as sulfoxides and/or sulfones, we should note that H_2O should be produced predominantly by the reduction of O_2 catalyzed by the vanadium complex without the formation of partially-reduced side products such as H_2O_2. The present paper reports a novel catalysis of the divanadium complex with salen ligands in the reduction of O_2 to H_2O with determination of the catalytic mechanism. The syntheses and the X-ray structures of the divanadium complexes are described, and the V(III)/O_2 chemistry is detailed. These results also provide an additional insight to the unique vanadium(III)/oxovanadium(V) redox chemistry with possible relevance to metal monooxygenases.

Experimental Section

Materials. All solvents were purified by distillation. Tetrabutylammonium tetrafluoroborate was obtained from Wako Chem. Co. and recrystallized from the mixture of benzene and ethyl acetate. (*N*,*N*′-Ethylenebis(salicylideneaminato))oxovanadium(IV) (VO(salen)), (*N*,*N*′-ethylenebis(salicylideneaminato))oxovanadium(V) tetrafluoroborate (VO(salen)BF_4), and (μ-oxo)bis[(*N*,*N*′-ethylenebis(salicylideneaminato))vanadium(IV)] tetrafluoroborate ([VOV(salen)$_2$][BF_4]$_2$, VOV^{2+}) (**I**) was prepared as previously described.[9]

Preparation of Compounds. A. [(salen)VOV(salen)][I_3] (II). Method 1: Reduction of I by Iodide. To a suspension of **I** (0.082 g, 0.1 mmol) in anhydrous CH_3CN (5 mL) was added tetrabutylammonium iodide (0.369 g, 1 mmol) under an atmosphere of pure argon. As the reducing agent dissolved, the color of the solution changed from dark red to dark green. After 4 h of stirring, the solvent was removed under vacuum, leaving a black residue. This residue was extracted with anhydrous CH_3CN (10 mL) under pure argon. Et_2O was diffused into the extract to yield the product **II** as dark red crystals. The product was identified by X-ray crystallography and elemental analysis. FTIR (KBr, cm^{-1}): 1616 ($\nu_{C=N}$), 978 ($\nu_{V=O}$). Anal. Calcd for $C_{32}H_{28}N_4O_5V_2I_3$: C, 37.27; H, 2.74; N, 5.43. Found: C, 35.80; H, 2.52; N, 5.71. NIR (ν_{max}, cm^{-1}, in CH_3CN): 7.1×10^3. UV (λ_{max}, nm, in CH_2Cl_2): 367, 280, 240. ESR (eight-line signal, in CH_2Cl_2): $g_0 = 1.98$, $A_0 = 100$ (G).

Method 2: Electroreduction of I. Electroreduction of **I** (2.1 mg, 0.0025 mmol) in CH_2Cl_2 (25 mL) with tetrabutylammonium tetrafluoroborate (0.82 g, 2.5 mmol) was performed by coulometric electrolysis at 0.3 V vs Ag/AgCl using a carbon felt as a working electrode. Removal of solvent followed by addition of tetrabutylammonium triiodide (0.016 g, 0.025 mmol) and crystallization from CH_3CN/Et_2O yielded the product **II** as dark red crystals which was identified as in Method 1.

Method 3. A procedure essentially identical to that described by Leigh et al.[10] was followed with slight modifications. A solution of I_2 (1.9 g, 7.5 mmol) in tetralin (70 mL) was added dropwise to boiling tetralin (40 mL) under an atmosphere of pure argon. The generated gaseous HI was introduced with argon to a green suspension of VO(salen) (2 g, 6 mmol) in anhydrous CH_3CN (50 mL). A small amount of I_2 contaminated in HI/argon proved to produce unidentified side products as brown solid; the amount of iodine in the gas was minimized by using the washing bottle cooled with dry ice which was placed before the reaction vessel. The suspension gradually turned dark brown. After all I_2 was added, the reaction mixture was refluxed for 30 min and then filtered to remove a little amount of brown solid. The filtrate was stored in a drybox under an atmosphere of pure argon at 20 °C. After 1 day, the produced dark red needles were collected, washed with anhydrous Et_2O, and dried *in vacuo*. The product was identified as in Method 1.

B. [(salen)VOVO(salen)][I_3] (III). O_2 gas was swept through a solution of **II** (0.011 g, 0.01 mmol) in CH_2Cl_2 (100 mL) for 1 day and then the solvent was replaced by CH_3CN (5 mL). Crystallization by vapor diffusion of Et_2O into the solution yielded dark brown plates of **III** in nearly quantitative yield as identified by X-ray crystallography and elemental analysis. FTIR (KBr, cm^{-1}): 1618 ($\nu_{C=N}$), 981 ($\nu_{V=O}$). Anal. Calcd for $C_{32}H_{28}N_4O_6V_2I_3$: C, 36.70; H, 2.69; N, 5.35. Found: C, 36.54; H, 2.60; N, 5.20. FABMS *(m/e)*: 1047. UV (λ_{max}, nm, in CH_2Cl_2): 365, 282, 240. ESR (eight-line signal, in CH_2Cl_2): $g_0 = 1.98$, $A_0 = 99.1$ (G).

C. [(salen)VOVO(salen)][ClO_4] (IV). The anhydrous 100 mL CH_2Cl_2 solution of **I** (0.0082 g, 0.01 mmol) with tetrabutylammonium perchlorate (3.42 g, 0.01 mol) was reduced by a carbon felt cathode at 0.3 V vs Ag/AgCl under an atmosphere of dry argon. After the coulometric reduction, O_2 gas was passed through the resulting solution for 1 day. Then the solvent was replaced by CH_3CN (5 mL). Slow diffusion of Et_2O into this solution caused the crystallization of the product as small black prisms of **IV** as identified by X-ray crystallography and elemental analysis. FTIR (KBr, cm^{-1}): 1093 (ν_{ClO_4}), 981 ($\nu_{V=O}$). Anal. Calcd for $C_{34}H_{31}ClN_5O_{10}V_2$: C, 50.61; H, 3.87; N, 8.68. Found: C, 50.20; H, 3.82; N, 8.32. UV (λ_{max}, nm, in CH_2Cl_2): 575, 371, 260, 190. ESR (eight-line signal, in CH_2Cl_2): $g_0 = 1.98$, $A_0 = 97.5$ (G).

Measurements. All measurements were performed in a drybox under an atmosphere of dry argon. Electrochemical measurements were carried out in a conventional two-compartment cell. A glassy carbon disk-platinum ring was used as a working electrode and polished before each experiment with 0.05-μm alumina paste. The auxiliary electrode, a coiled platinum wire, was separated from the working solution by a fine-porosity frit. The reference electrode was a commercial Ag/AgCl electrode immersed in a salt bridge consisting of 0.1 mol/L tetrabutylammonium tetrafluoroborate, which was placed in a main cell compartment. The formal potential of the ferrocene/ferrocenium couple in dichloromethane was 0.34 V vs this reference electrode. All potentials are quoted with respect to this Ag/AgCl reference electrode. A Nikko Keisoku DPGS-1 dual potentiogalvanostat and a Nikko Keisoku NFG-3 universal programmer were employed with a Graphtec WX2400 X-Y recorder to obtain the voltammograms. Coulometric exhaustive electrolysis was performed using a Nikko Keisoku NDCM-1 digital coulomb meter. UV-vis spectra were obtained using a Shimadzu UV-2100 spectrophotometer. Infrared spectra were obtained using a JASCO FT-IR 5300 as potassium bromide pellets. Near-infrared spectra were obtained using a Shimadzu UV3101PC spectrophotometer. A quartz-glass cell with 0.2-cm optical path length was employed. FABMS spectrum was obtained using a VGZAB-HF Spectrometer with *m*-nitrobenzyl alcohol as the matrix material.

X-ray Crystallography. Dark red needle crystals of **II** and black prismatic crystals of **III** and **IV** were grown from acetonitrile solutions of the desired complexes after layering with ether. Following microscopic examination in air in each case, a suitable crystal was mounted on a glass fiber at room temperature. All measurements were made on a Rigaku AFC5R diffractometer with a 7.5 kW rotating anode generator and graphite monochromated MoKα radiation ($\lambda = 0.71069$

(7) (a) Tsuchida, E.; Yamamoto, K.; Jikei, M.; Nishide, H. *Macromolecules* **1989**, *22*, 4138. (b) Yamamoto, K.; Tsuchida, E.; Nishide, H.; Jikei, M.; Oyaizu, K. *Macromolecules* **1993**, *26*, 3432. (c) Tsuchida, E.; Yamamoto, K.; Oyaizu, K.; Suzuki, F.; Nishide, H.; Hay, A. S.; Wang, Z. Y. *Macromolecules* **1995**, *28*, 409. (d) Oyaizu, K.; Iwasaki, N.; Yamamoto, K.; Nishide, H.; Tsuchida, E. *Bull. Chem. Soc. Jpn.* **1994**, *67*, 1456. (e) Yamamoto, K.; Jikei, M.; Oyaizu, K.; Suzuki, F.; Nishide, H.; Tsuchida, E. *Bull. Chem. Soc. Jpn.* **1994**, *67*, 251.

(8) (a) Patel, K. S.; Kolawole, G. A. *J. Coord. Chem.* **1986**, *15*, 137. (b) Selbin, J. *Chem. Rev.* **1965**, *65*, 153. (c) Selbin, *J. Coord. Chem. Rev.* **1966**, *1*, 293.

(9) Tsuchida, E.; Yamamoto, K.; Oyaizu, K.; Iwasaki, N.; Anson, F. C. *Inorg. Chem.* **1994**, *33*, 1056.

(10) Hughes, D. L.; Kleinkes, U.; Leigh, G. J.; Maiwald, M.; Sanders, J. R.; Sudbrake, C. *J. Chem. Soc., Dalton Trans.* **1994**, 2457.

Table 1. Summary of X-ray Crystallographic Data

complex	[(salen)VOV(salen)][I_3] (**II**)	[(salen)VOVO(salen)][I_3] (**III**)	[(salen)VOVO(salen)][ClO_4] (**IV**)
emp form	$C_{32}H_{28}N_4O_5V_2I_3$	$C_{32}H_{28}N_4O_6V_2I_3$	$C_{34}H_{31}ClN_5O_{10}V_2$
fw	2062.39	1047.19	806.98
cryst syst	triclinic	triclinic	triclinic
space group	$P\bar{1}$ (no. 2)	$P\bar{1}$ (no. 2)	$P\bar{1}$ (no. 2)
a (Å)	13.436(4)	14.973(2)	11.923(3)
b (Å)	13.969(4)	19.481(2)	14.25(1)
c (Å)	12.046(4)	14.168(2)	11.368(7)
α (deg)	104.47(3)	107.00(1)	112.92(5)
β (deg)	115.98(2)	115.56(1)	92.76(4)
γ (deg)	97.77(3)	80.35(1)	99.13(4)
V (Å^3)	1888(1)	3561.3(9)	1743(1)
Z	2	4	2
density (calcd)	1.813 g/cm^3	1.953 g/cm^3	1.537 g/cm^3
crystal size (mm)	0.2 × 0.1 × 0.4	0.4 × 0.1 × 0.3	0.2 × 0.2 × 0.1
radiation	MoKα (λ = 0.71069 Å)	MoKα (λ = 0.71069 Å)	CuKα (λ = 1.54178 Å)
absn coeff μ	28.82 cm^{-1}	31.74 cm^{-1}	57.59 cm^{-1}
2θ max (deg)	50.0	50.0	110.1
no. of reflns colld	6957	13070	4595
no. of unq reflns	6646	12541	4377
no. of obsd reflns	3760 ($I > 3.00\sigma(I)$)	6584 ($I > 3.00\sigma(I)$)	3089 ($I > 3.00\sigma(I)$)
params	415	847	497
refln/param ratio	9.06	7.77	6.22
R	0.086	0.057	0.042
R_w	0.119	0.065	0.061
goodness-of-fit	1.67	1.35	1.58
max peak in diff map	5.34 e$^-$/Å^3	2.67 e$^-$/Å^3	0.40 e$^-$/Å^3
min peak in diff map	−3.91 e$^-$/Å^3	−1.25 e$^-$/Å^3	−0.37 e$^-$/Å^3

Å) for **II** and **III** and with a 12 kW rotating anode generator and graphite monochromated CuKα radiation (λ = 1.54178 Å) for **IV**. Unit cell parameters and an orientation matrix for data collection were determined by least-squares refinements using the setting angles of 25 carefully centered reflections in the range $20 < 2\theta < 25°$ for **II** and **III**, and in $40 < 2\theta < 41°$ for **IV**. The data were collected at a temperature using the $\omega-2\theta$ scan technique to a maximum 2θ value of 55° for **II** and **III** and of 110° for **IV**. Scans were made at a speed of 8°/min (in omega) for **II** and **IV** and at 16°/min (in omega) for **III**. The weak reflections ($I < 3\sigma(I)$ for **II** and **III** and $I < 15\sigma(I)$ for **IV**) were rescanned (up to 2 scans) and the counts were accumulated to ensure good counting statistics. Stationary background counts were recorded on each side of the reflection. The ratio of peak counting time to background counting time was 2:1. The diameter of the incident beam collimator was 1.0 mm. The crystal to detector distance was 258 nm, and the computer controlled detector aperture was set to 9 × 13 mm (horizontal × vertical). The intensities of three representative reflection were measured after every 200 reflections. No decay correction was applied. The data were corrected for Lorentz and polarization effects.

Structure Solution and Refinement. The structure was solved by heavy-atom Patterson methods and expanded using Fourier techniques. Positions for most non-hydrogen atoms were visible on the initial *E*-map with positions of the remaining atoms found on subsequent electron density difference maps. The nonhydrogen atoms were refined anisotropically. Hydrogen atoms were included but not refined. The final cycle of full-matrix least-squares refinement[11] was based on observed reflections ($I > 3\sigma(I)$) and converged with unweighted and weighted agreement factors of $R = \sum||F_o| - |F_c||/\sum|F_o|$ and $R_w = (\sum w(|F_o| - |F_c|)^2/\sum wF_o^2)^{1/2}$ as listed in Table 1. Plots of $\sum w(|F_o| - |F_c|)^2$ versus $|F_o|$, reflection order in data collection, $\sin\theta/\lambda$ and various classes of indices showed no unusual trends. Data collection and structure solution parameters and conditions are listed in Table 1. Selected bond lengths and angles for **III** are listed in Tables 2 and 3, respectively, and those for **IV** are listed in Tables 4 and 5, respectively.

(11) Least-squares: Function minimized: $\sum w(|F_o| - |F_c|)^2$, where $w = (\sigma(F_o)^2 + (0.020(F_o))^2)^{-1}$.

(12) teXsan: Crystal Structure Analysis Package; Molecular Structure Corporation: 1985 & 1992.

(13) (a) Riley, P. E.; Pecoraro, V. L.; Carrano, C. J.; Bonadies, J. A.; Raymond, K. N. *Inorg. Chem.* **1986**, *25*, 154. (b) Bonadies, J. A.; Butler, W. M.; Pecoraro, V. L.; Carrano, C. J. *Inorg. Chem.* **1987**, *26*, 1218.

Table 2. Selected Bond Lengths for [(salen)VOVO(salen)][I_3] (**III**) Characterized by X-ray Crystallography

atom−atom	bond length	atom−atom	bond length
V(1)−O(1)	1.90(1)	V(1)−O(2)	1.894(8)
V(1)−O(3)	1.623(6)	V(1)−N(1)	2.02(1)
V(1)−N(2)	2.04(1)	V(2)−O(3)	2.214(6)
V(2)−O(4)	1.83(1)	V(2)−O(5)	1.811(7)
V(2)−O(6)	1.573(7)	V(2)−N(3)	2.07(1)
V(2)−N(4)	2.08(1)	V(3)−O(7)	1.928(8)
V(3)−O(8)	1.90(1)	V(3)−O(9)	1.613(7)
V(3)−N(5)	2.05(1)	V(3)−N(6)	2.065(9)
V(4)−O(9)	2.246(7)	V(4)−O(10)	1.85(1)
V(4)−O(11)	1.823(8)	V(4)−O(12)	1.578(7)
V(4)−N(7)	2.08(1)	V(4)−N(8)	2.11(1)

[a] Bond lengths are in Å. Estimated standard deviations are given in parentheses.

All calculations were performed using the teXsan crystallographic software package of Molecular Structure Corporation.[12]

Results and Discussion

Synthesis, Structure and Redox State of a μ-Oxo Divanadium Complex (II). Electrochemical and structural studies of oxovanadium complexes with Schiff-base ligands attract particular attention because of their reversible one-electron redox behaviors allowing possible applications to electrocatalysts. VO(salen) and its oxidized product V^VO(salen)ClO_4 crystallize easily and their X-ray structures have been solved.[13] The (μ-oxo)divanadium(IV) complex [(salen)VOV(salen)][BF_4]$_2$ (**I**) can be prepared as a black powder by the acidification of VO(salen) with trifluoromethanesulfonic acid or trityl tetrafluoroborate in nonaqueous media ($2VO(salen) + 2H^+ \rightarrow VOV^{2+} + H_2O$) as previously described.[9] Attempts to obtain single crystals of **I** met with failure. Reasoning that the isolation of **I** might be disfavored in CH_3CN most amenable for crystallization because of the dissociation equilibrium with mononuclear complexes,[9] we turned to the reduced complex of **I**.

The reduction of **I** by tetrabutylammonium iodide (method 1) produced a mixed-valent, μ-oxo divanadium(III, IV) complex [(salen)$V^{IV}OV^{III}$(salen)][I_3] (**II**). X-ray analysis revealed the

Table 3. Selected Bond Angles for [(salen)VOVO(salen)][I_3] (**III**) Characterized by X-ray Crystallography

atom−atom−atom	angle	atom−atom−atom	angle
O(1)−V(1)−O(2)	88.5(4)	O(1)−V(1)−O(3)	106.1(4)
O(1)−V(1)−N(1)	87.2(4)	O(1)−V(1)−N(2)	149.8(3)
O(2)−V(1)−O(3)	110.8(4)	O(2)−V(1)−N(1)	144.4(3)
O(2)−V(1)−N(2)	87.7(4)	O(3)−V(1)−N(1)	104.4(4)
O(3)−V(1)−N(2)	103.3(4)	N(1)−V(1)−N(2)	78.8(5)
O(3)−V(2)−O(4)	83.4(3)	O(3)−V(2)−O(5)	82.8(3)
O(3)−V(2)−O(6)	174.0(5)	O(3)−V(2)−N(3)	81.7(3)
O(3)−V(2)−N(4)	79.0(3)	O(4)−V(2)−O(5)	106.8(4)
O(4)−V(2)−O(6)	98.8(4)	O(4)−V(2)−N(3)	86.4(4)
O(4)−V(2)−N(4)	156.5(3)	O(5)−V(2)−O(6)	101.8(4)
O(5)−V(2)−N(3)	158.3(4)	O(5)−V(2)−N(4)	86.3(4)
O(6)−V(2)−N(3)	92.9(4)	O(6)−V(2)−N(4)	97.3(5)
N(3)−V(2)−N(4)	75.9(4)	O(7)−V(3)−O(8)	90.3(4)
O(7)−V(3)−O(9)	105.3(4)	O(7)−V(3)−N(5)	87.1(4)
O(7)−V(3)−N(6)	149.3(3)	O(8)−V(3)−O(9)	107.7(5)
O(8)−V(3)−N(5)	146.7(4)	O(8)−V(3)−N(6)	88.0(4)
O(9)−V(3)−N(5)	105.0(5)	O(9)−V(3)−N(6)	104.4(4)
N(5)−V(3)−N(6)	77.9(4)	O(9)−V(4)−O(10)	82.7(3)
O(9)−V(4)−O(11)	82.4(3)	O(9)−V(4)−O(12)	175.8(4)
O(9)−V(4)−N(7)	83.8(3)	O(9)−V(4)−N(8)	80.0(4)
O(10)−V(4)−O(11)	109.0(5)	O(10)−V(4)−O(12)	97.5(4)
O(10)−V(4)−N(7)	85.5(4)	O(10)−V(4)−N(8)	156.0(3)
O(11)−V(4)−O(12)	101.4(4)	O(11)−V(4)−N(7)	158.4(5)
O(11)−V(4)−N(8)	85.1(5)	O(12)−V(4)−N(7)	92.0(4)
O(12)−V(4)−N(8)	98.5(5)	N(7)−V(4)−N(8)	76.2(4)
V(1)−O(3)−V(2)	166.6(5)	V(3)−O(9)−V(4)	162.8(6)

[a] Angles are in degrees. Estimated standard deviations are given in parentheses.

Table 4. Selected Bond Lengths for [(salen)VOVO(salen)][ClO_4] (**IV**) Characterized by X-ray Crystallography

atom−atom	bond length	atom−atom	bond length
V(1)−O(1)	1.910(3)	V(1)−O(2)	1.899(3)
V(1)−O(3)	1.618(3)	V(1)−N(1)	2.042(3)
V(1)−N(2)	2.056(4)	V(2)−O(3)	2.250(3)
V(2)−O(4)	1.822(3)	V(2)−O(5)	1.809(3)
V(2)−O(6)	1.597(4)	V(2)−N(3)	2.081(4)
V(2)−N(4)	2.091(4)		

[a] Bond lengths are in Å. Estimated standard deviations are given in parentheses.

Table 5. Selected Bond Angles for [(salen)VOVO(salen)][ClO_4] (**IV**) Characterized by X-ray Crystallography

atom−atom−atom	angle	atom−atom−atom	angle
O(1)−V(1)−O(2)	89.5(1)	O(1)−V(1)−O(3)	105.9(2)
O(1)−V(1)−N(1)	86.4(1)	O(1)−V(1)−N(2)	148.9(1)
O(2)−V(1)−O(3)	110.2(1)	O(2)−V(1)−N(1)	144.9(1)
O(2)−V(1)−N(2)	87.8(2)	O(3)−V(1)−N(1)	104.5(2)
O(3)−V(1)−N(2)	104.0(1)	N(1)−V(1)−N(2)	78.3(1)
O(3)−V(2)−O(4)	82.5(1)	O(3)−V(2)−O(5)	84.1(1)
O(3)−V(2)−O(6)	173.0(1)	O(3)−V(2)−N(3)	82.2(1)
O(3)−V(2)−N(4)	77.2(1)	O(4)−V(2)−O(5)	106.7(1)
O(4)−V(2)−O(6)	99.4(2)	O(4)−V(2)−N(3)	86.0(1)
O(4)−V(2)−N(4)	155.0(1)	O(5)−V(2)−O(6)	101.7(2)
O(5)−V(2)−N(3)	159.9(2)	O(5)−V(2)−N(4)	85.8(1)
O(6)−V(2)−N(3)	91.2(2)	O(6)−V(2)−N(4)	99.1(2)
N(3)−V(2)−N(4)	76.9(1)	V(1)−O(3)−V(2)	169.1(2)

[a] Angles are in deg. Estimated standard deviations are given in parentheses.

molecular structure of the complex as a triiodide salt as shown in Figure 1. As an alternative reduction method, controlled potential reduction of the dimer **I** at 0.3 V was carried out (method 2). The redox potential of the complex **I** is located at 0.44 V vs Ag/AgCl in CH_2Cl_2,[14] and controlled potential reduction at 0.3 V under N_2 consumed one electron per mole

(14) The formal potential of the ferrocene/ferrocenium complex was 0.34 V vs this reference electrode. All potentials are quoted to this Ag/AgCl reference electrode.

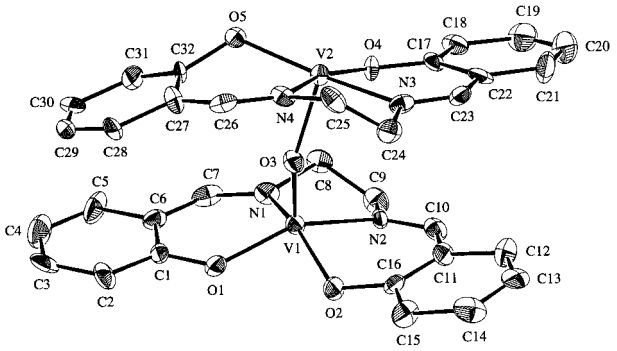

Figure 1. ORTEP view (50% probability ellipsoids) of a cation in [(salen)VOV(salen)][I_3] **(II)**.

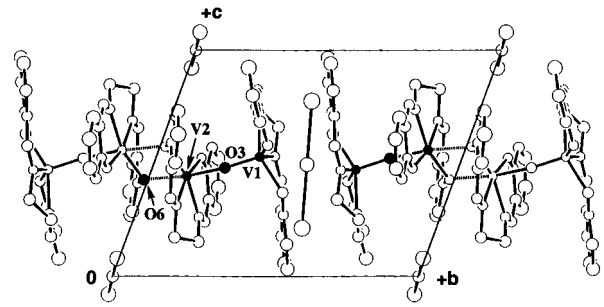

Figure 2. ORTEP diagram of the unit cell of **II** viewed down the *a*-axis.

of complex as expected for quantitative reduction to VOV^+ (eq 1).[9]

$$[(\text{salen})V^{IV}OV^{IV}(\text{salen})]^{2+} + e^- \rightarrow [(\text{salen})V^{IV}OV^{III}(\text{salen})]^+ \quad (1)$$

The crystallization of the reduced species was performed in CH_3CN/Et_2O in the presence of added tetrabutylammonium salts such as perchlorate, hexafluorophosphate, bromide, iodide, and triiodide. Good crystals were obtained only for the triiodide salt.

The crystal structure of **II** was essentially the same as that reported by Leigh et al.[10] The previous study[10] involved the addition of HI to solutions of VO(salen) in acetonitrile. We could also obtain the complex **II** by the analogous method with slight modifications (method 3). It can be reasoned that acidification of VO(salen) with HI would first result in dimerization of VO(salen)[9] and then in subsequent reduction by iodide to produce **II**. The phenolate oxygen in a salen ligand often serves as a bridging ligand; the typical example is provided by Cu(salen) which crystallizes in a dimeric arrangement with nonplanarity of the central coordinated group.[15] Indeed, the molecular structure of **II** can also be taken as tetravanadium complex, as in the previous work,[10] with the center of symmetry being located at the center of the molecule (Figure 2). But since O(6) in the adjacent cation is located as long as 2.101(9) Å beyond V(2), and O(5) deviates from the N(3)N(4)O(4) plane by only 0.472 Å, the cation structure can be regarded as a dinuclear complex, rather than a tetranuclear complex, with O(5) and O(6) axially located near vanadium in the octahedral arrangement. It is known that vanadium(III) prefers an octahedral arrangement, whereas vanadium(IV) is more stable in square pyramidal geometry. The V(2) atom in the monocation structure, surrounded by the four-coordinating atoms of a salen ligand, extends only 0.059 Å above the best N_2O_2 least-square plane with O(3)−V(2)−O(6) angle of 170.4(4)°. The arrange-

(15) Hall, D.; Waters, T. N. *J. Chem. Soc.* **1960**, 2644.

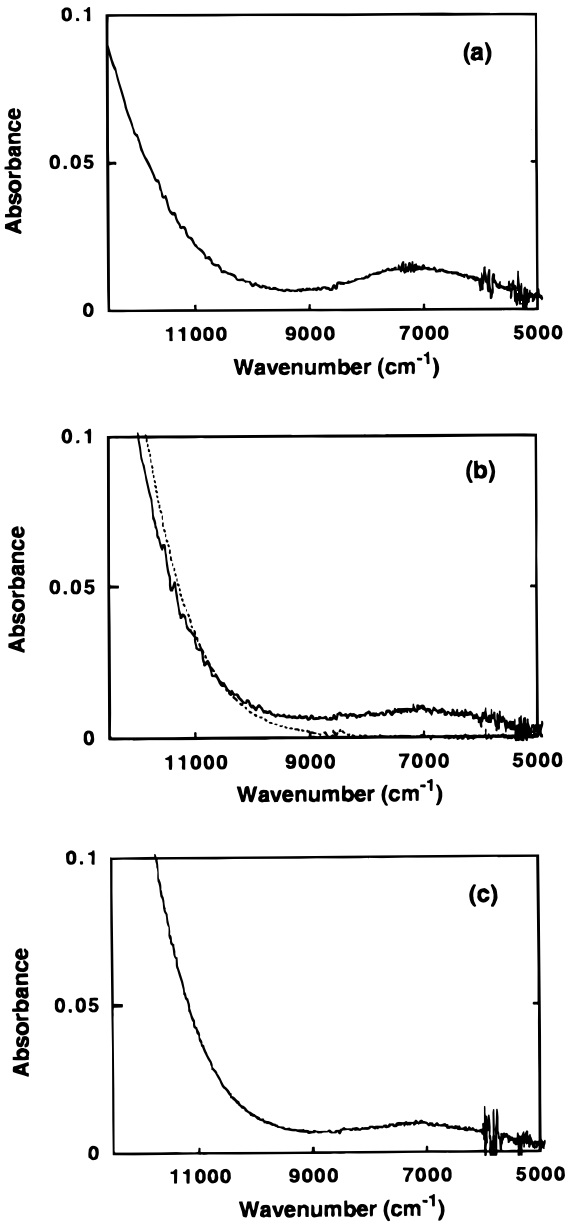

Figure 3. Near-infrared spectra of solutions prepared by dissolving (a) 5.0 mmol/L divanadium(III, IV) complex (**II**); (b) 5.0 mmol/L divanadium (IV, V) complex (**III**) (dotted curve), 5.0 mmol/L **III** + 10 mmol/L CF_3SO_3H (solid curve); (c) 5.0 mmol/L divanadium complex (**I**) + 0.1 mol/L tetrabutylammonium tetrafluoroborate following controlled potential oxidation at 0.7 V which consumed one electron per molecule of dimer. The solvent was anhydrous CH_3CN. Optical path length = 0.2 cm. The baselines are corrected by subtracting the spectrum of CH_3CN.

ment around V(2) is pseudo octahedral. In contrast, V(1) atom lying as far as 0.534 Å above the N_2O_2 plane and O(3) 1.646(10) Å beyond the V(1) atom represent a typical square-pyramidal coordination arrangement. The bond length of the vanadium atom and the equatorial phenolate oxygen of the ligand are indicative of the oxidation state, since the V−O(phenolate) bond is known to shrink as the vanadium is oxidized. The V(1)−O(phenolate) bond length (V(1)−O(1), 1.885(9) Å; V(1)−O(2), 1.927(9) Å) is shorter than that of V(2)−O(phenolate) bond length (V(2)−O(4), 1.890(9) Å; V(2)−O(5), 1.941(10) Å). Thus V(1) and V(2) are ascribed to vanadium(IV) and vanadium(III), respectively.

The mixed-valent state was characterized by the near-infrared spectrum of **II** as shown in Figure 3(a). An intervalence

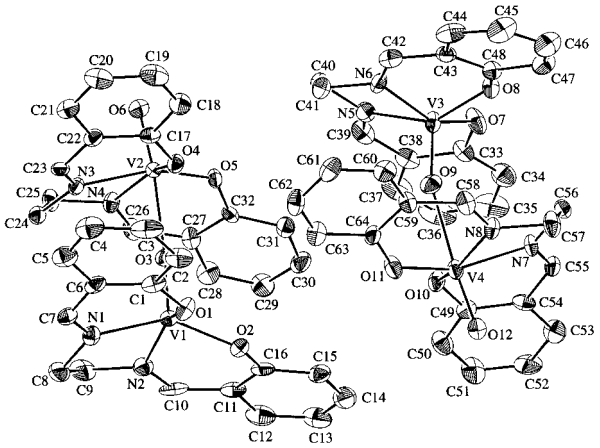

Figure 4. ORTEP view (30% probability ellipsoids) of cations in asymmetric unit of [(salen)VOVO(salen)][I_3] **(III)**.

transition band was observed at $\nu_{max} = 7.2 \times 10^3$ cm^{-1} in acetonitrile with half band width $\Delta_{1/2}$ of 3.0×10^3 cm^{-1} and molar absorption coefficient ϵ_{max} of 60.1 M^{-1} cm^{-1} at the ν_{max}.[16] The crystal structure provided the non-bonding vanadium(III)-to-vanadium(IV) distance of 3.569(4) Å in the dinuclear complex. The interaction factor α of the mixed valent state was determined to be 3.0×10^{-2}.[17] The complex **II** was classified into a Type II mixed-valent complex: The optical and electronic properties of **II** are based not only on the constituent components but also on their interaction.[18]

Syntheses and Structures of Divanadium Complexes (III, IV). It is well-known that the reactivity of vanadium complexes toward O_2 is responsive to the redox state and the coordination structure. A typical example is provided by acetylacetonate complexes: a six-coordinate vanadium(III) complex $V(acac)_3$ is oxidized by O_2 whereas a five-coordinate vanadium(IV) complex, $VO(acac)_2$, is stable in air. The structure of **II** containing the five-coordinate vanadium(III) prompted us to examine the reaction with O_2. The oxidation of **II** by O_2 in anhydrous CH_2Cl_2 proceeded almost stoichiometrically to produce a divanadium(IV, V) complex **(III)**.[19] The crystallization of **III** was performed in CH_3CN/Et_2O to produce dark brown crystals. X-ray diffraction studies of the crystallized product revealed the formation of [(salen)VOVO(salen)][I_3] complex (Figure 4). The structure consists of two crystallographically independent molecules per asymmetric unit. The V(2) and V(4) atom, surrounded by the four coordinating atoms of a salen ligand (N_2O_2), extends 0.270 Å and 0.262 Å, respectively, above the best N_2O_2 least-squares plane. The

(16) Our previous study (reference 9) revealed that the μ-oxo divanadium cation is substantially dissociated in acetonitrile solutions. The dissociation equilibrium of the divanadium(III, IV) complex has been established as K = [VO(salen)][V(salen)$^+$]/[(salen)VOV(salen)$^+$] = 13 mM. The molar absorption coefficient of the intervalence transition band was determined with regard to the equilibrium concentration of the undissociated dimer which is responsible for the electronic transition concerned.

(17) (a) $\alpha^2 = (4.5 \times 10^{-4})\epsilon_{max}\Delta_{1/2}\nu^{-1}r^{-2}$, where α is the interaction parameter and r is the distance separating the interacting donor-acceptor moieties. The extent of interaction is defined for the ground state of the complex as $\psi_G = (1-\alpha^2)^{1/2}\phi_i + \alpha\phi_j$ where ϕ_i and ϕ_j are wave functions for the donor-acceptor components of the mixed-valence system. Cowan, D. O.; Vanda, C. L.; Park, J.; Kaufman, F. *Acc. Chem. Res.* **1973**, *6*, 1. (b) Allen, G. C.; Hush, N. S. *Prog. Inorg. Chem.* **1967**, *8*, 357. (c) Hush, N. S. *Prog. Inorg. Chem.* **1967**, *8*, 391. (d) Hush, N. S. *Coord. Chem. Rev.* **1985**, *64*, 135.

(18) Robin, M. B.; Day, P.; *Adv. Inorg. Chem. Radiochem.* **1967**, *10*, 247.

(19) The oxidation of **II** by O_2 obeyed a rate law pseudo second-order in **II**, which suggested a mechanism of oxidation involving a bimolecular reaction to produce an O_2-adduct such as peroxo tetramer as the rate limiting step. The homolytic scission of the intermediate is a likely reaction to generate two molecules of the $VOVO^+$ cation.

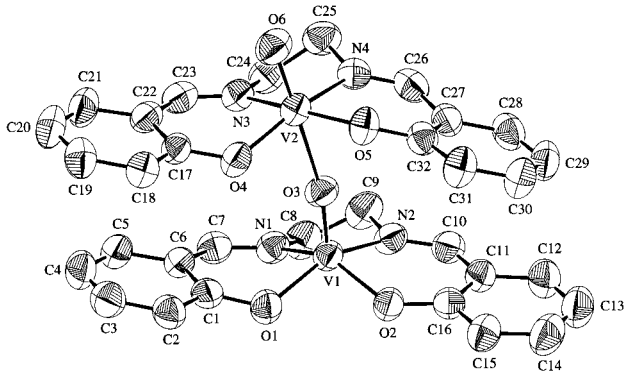

Figure 5. ORTEP view (50% probability ellipsoids) of a cation in [(salen)VOVO(salen)][ClO_4] **(IV)**.

arrangement around V(2) and V(4) is fairly distorted octahedral. In contrast, V(1) atom lying as far as 0.550 Å above the N_2O_2 plane and O(3) being 1.622(7) Å beyond the V(1) atom represent a typical square-pyramidal coordination structure. The V(2) atom deviating from the N_2O_2 plane by 0.536 Å also represents a square-pyramidal arrangement. It is known that the oxovanadium average V═O bond length is approximately 1.6 Å and the oxidation state of the vanadium atom is hardly reflected in this. Nevertheless, we notice that the 1.573(8)-Å V(2)−O(6) distance and the 1.578(8)-Å V(4)−O(12) distance are closer to the V═O bond length of oxovanadium(V) complexes such as those of VO(salen)ClO_4 (1.576(3) Å) and VO(salen)BF_4 (1.577-(1) Å) than to that of $V^{IV}O$(salen) (1.583(5) Å). The bond length of the vanadium atom and the phenolate oxygen of the ligand are again indicative of the oxidation state. The shorter V−O(phenolate) bond length around V(2) and V(4), and the longer length around V(1) and V(3) (Table 2) support the $[V^{IV}-O-V^{V}=O]^+$ oxidation state. It may be the preference of vanadium(V) to be six coordinate rather than five coordinate that drives the formation of the $VOVO^+$ cation. The weak axial interaction with O(3) and O(9), as judged by the long V(2)−O(3) and V(4)−O(9) bond length and the substantial deviations of the V(2) and V(4) atoms from the N_2O_2 plane, are due to the low residual basicity of O(3) and O(9) which are already bound to vanadium(IV). The units of the two molecules are separated by the almost linear I_3^- anion which is arranged between the unit.

It follows that the VOV^+ complex, produced by the stoichiometric electroreduction of **I** (eq 1), is also expected to give $VOVO^+$ cation by O_2-oxidation. Thus, a solution of **I** in anhydrous CH_2Cl_2 containing 0.1 M tetrabutylammonium perchlorate was subjected to controlled potential reduction at 0.3 V under N_2 to prepare the solution of VOV^+, and the resulting solution was exposed to O_2 gas. The oxygenated product was crystallized after solvent-exchange with CH_3CN/Et_2O and allowing the solution to stand for several days. X-ray diffraction studies of the crystallized product **IV** revealed the composition of $[(salen)VOVO(salen)]^+$ cation (Figure 5), ClO_4^- anion, and CH_3CN.

$$2[(salen)V^{IV}-O-V^{III}(salen)]^+ + O_2 \rightarrow 2[(salen)V^{IV}-O-V^{V}(salen)=O]^+ \quad (2)$$

In the cation structure of **IV**, the V(1) atom lay out of the best N_2O_2 least-squares plane by 0.553 Å, representing a square-pyramidal coordination structure. The arrangement around V(2), deviating 0.274 Å from the N_2O_2 plane, is distorted octahedral. The V−O(phenolate) bond length again suggests the valence state as $[V^{IV}-O-V^{V}=O]^+$. Aside from the cation structure of **IV** being very similar to that of **III**, the arrangement of the perchlorate anion indicates an absence of vanadium-perchlorate interaction, in contrast to the monomeric $[V^{V}O(salen)][ClO_4]$[13] in which perchlorate is located in the proximity of the square-pyramidal vanadium(V) atom with V−O(perchlorate) distance of 2.456(3) Å. A comparison of the two structures suggest that the contact between the perchlorate anion and the vanadium atom is more impeded in **IV** containing six-coordinated vanadium(V) and square-pyramidal vanadium(IV).

The stoichiometry of reaction 2 is reminiscent of the electroreduction of O_2 to H_2O. It is of interest that oxygenation of vanadium(III) gives oxovanadium(V), whereas multiple one-electron redox centers have been considered to be essential for the incorporation of O_2. An explanation for this can be found in the high reactivity of the five-coordinate vanadium(III) and the stability of the oxovanadium(V) species.

Deoxygenation of III and IV. It has been confirmed that $V^{IV}O$(salen) undergoes deoxygenation to give V(salen)$^{2+}$ and H_2O in strongly acidic conditions.[9] The reactivity of **II** toward O_2 (eq 2), with significant potential in leading to the selective four-electron reduction of O_2 to H_2O, prompted the study on the reaction of the $[(salen)VOVO(salen)]^+$ cation with a strong acid to undergo deoxygenation of the $VOVO^+$ cation to VOV^{3+} species. As expected, the V═O stretching bands in the infrared spectrum of **III** and **IV** (981 cm^{-1}) disappeared when 2-fold mole of CF_3SO_3H was added to the CH_3CN solution. The vanadium species produced in the presence of protons may be attributable to $[(salen)VOV(salen)]^{3+}$. The deoxygenation reaction believed to be responsible for the generation of $[(salen)VOV(salen)]^{3+}$ from $[(salen)VOVO(salen)]^+$ is

$$[(salen)VOVO(salen)]^+ + 2H^+ \rightarrow [(salen)VOV(salen)]^{3+} + H_2O \quad (3)$$

Although the crystallization of $[(salen)VOV(salen)]^{3+}$ complex was unsuccessful, probably due to the enhanced reactivity, the cation was detected in the mass spectrum (*m/z*: 651). Moreover, the resulting acidic solution exhibited a weak intervalence transition band in the near-infrared spectrum as shown in Figure 3(b) with ν_{max} of 7.1×10^3 cm^{-1}, $\Delta_{1/2}$ of 3.2×10^3 cm^{-1} and ϵ_{max} of 10 M^{-1} cm^{-1} at the ν_{max}. Our previous study[9] revealed that $[(salen)V^{IV}OV^{V}(salen)]^{3+}$ cation is produced by coulometric one-electron oxidation of **I**. Added support for deoxygenation was provided by a good agreement between the near-infrared spectra of the $[(salen)VOV(salen)]^{3+}$ solution (Figure 3(c)) and that of the solution of the $VOVO^+$ cations after treatment with CF_3SO_3H. Agreement between the UV-vis. spectra was also confirmed ($\lambda_{max} = 245$ nm, $\epsilon_{max} = 6.8 \times 10^4$ M^{-1} cm^{-1}). While the lack of X-ray data prevents further determination of the electronic states, the formation of a mixed-valent $[(salen)V^{IV}OV^{V}(salen)]^{3+}$ cation is evidenced by means of those spectroscopic measurements.

Homogeneous Catalysis of the Electroreduction of O_2. In attempts to develop catalytic reduction of O_2, the vanadium complex **I** with the well-defined catalytic cycle was employed as a mediator. The electroreduction of O_2 was performed with the complex **I** in CH_2Cl_2 containing trifluoroacetic acid. Cyclic voltammograms for the electroreduction of O_2 at graphite electrodes are shown in Figure 6(a). As expected, a large catalytic current was observed at $E_p = 0.17$ V vs Ag/AgCl. The reduction of O_2 seems to begin near the redox potential of **I** (0.44 V vs Ag/AgCl). To elucidate more quantitatively the stoichiometry of the reduction of O_2, a rotating ring-disk electrode was employed.[20] Collection experiments of H_2O_2 at

(20) Bard, A. J.; Faulkner, L. R. *Electrochemical Methods*; John Wiley & Sons: New York, 1980; Chapter 8.

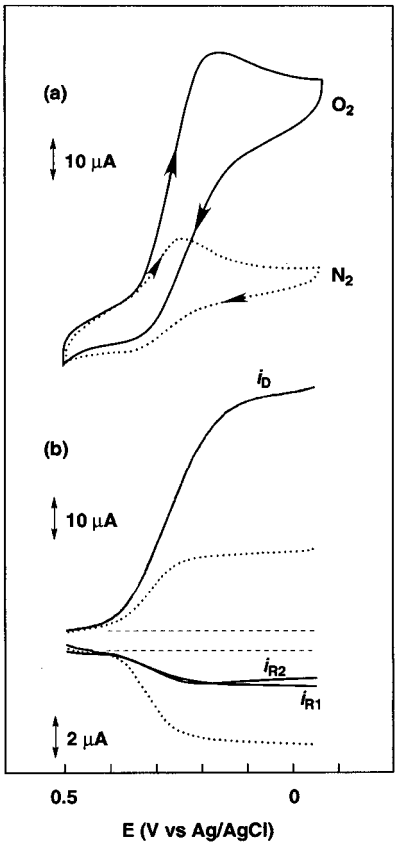

Figure 6. (a) Cyclic voltammogram obtained for a solution prepared by dissolving 0.5 mmol/L of **I** in anhydrous CH_2Cl_2 saturated with O_2 or N_2 in the presence of 0.1 mol/L trifluoroacetic acid at glassy carbon electrode (ϕ = 6 mm); supporting electrolyte = 0.1 mol/L tetrabutylammonium tetrafluoroborate; scan rate = 50 mV/s. (b) Rotating ring-disk voltammogram in the same solution using a platinum ring-glassy carbon disk electrode; the solid curves were recorded under O_2 and the dotted curves under N_2; rotating speed = 100 rpm; scan rate = 5 mV/s; disk current shown above, ring current below, the *x* axis. Ring potential: dotted curve (under N_2), +0.5V; solid curve (under O_2) i_{R1}, +0.5V; i_{R2}, +1.4 V. The potentials are referenced against Ag/AgCl. The anodic wave for the oxidation of H_2O_2 in acidic CH_2Cl_2 was at E_p = +1.3 V vs this Ag/AgCl.

the ring electrode (i_{R2}) revealed that the vanadium complex resulted in a catalysis to allow four-electron reduction of O_2 to H_2O predominantly. The ratio of the ring to disk currents (i_{R2}/i_D) in Figure 6(b) corresponds to the reduction of more than 90% of the O_2 molecules to H_2O.[21] The complex **I** showed virtually no catalytic activity for the reduction of H_2O_2, which indicate that a small amount of H_2O_2 is formed only as a parallel product in O_2 reduction, not as an intermediate.[22] Thus the complex **I** proved to be an effective electrocatalyst for the direct four-electron reduction of O_2 to H_2O.[23]

The need for the four-electron reduction of O_2 as pointed out earlier is the capacity of forming an intercalated peroxo complex such as the Co−O−O−Co complex using the difacial cobalt porphyrins and the dimeric iridium porphyrin.[3] In recent studies, Anson and co-workers have demonstrated that the coordination of more than two $Ru(NH_3)_5$ groups to the meso pyridine ligands of the cobalt porphyrin ring is effective in accessing the four-electron reduction pathway.[4] The use of oxovanadium complex proved valuable in this study though it remains to be determined how protons take part in the oxygenation of vanadium to accelerate the overall catalytic reaction. Nevertheless under conditions where oxygenation of vanadium(III) to oxovanadium(V) followed by acid-promoted deoxygenation proceeds, a reasonable yield of H_2O was obtained in the electroreduction of O_2. Since the oxygenation-deoxygenation process of vanadium(III) yields two-electron-oxidized vanadium(V), it can be stated that the one-step two-electron redox couple of $[(salen)VOV(salen)]^{3+/+}$ which can transfer isoenergetically two electrons plays an essential role on the catalytic activity.

Scheme 1

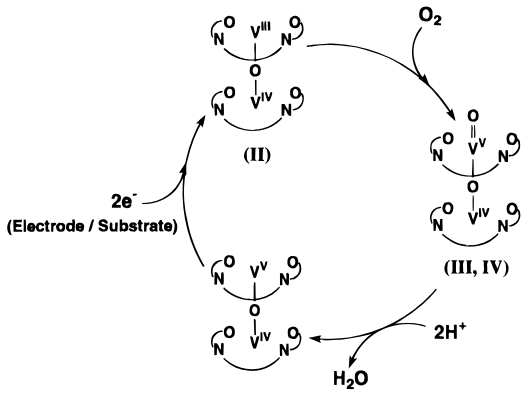

Conclusions

We report herein the discovery of a catalytic cycle containing $[(salen)VOV(salen)]^+$ **(II)** and $[(salen)VOVO(salen)]^+$ **(III, IV)**, well-defined electrocatalysts for the four-electron reduction of O_2. This result encourages us to postulate that a similar catalytic cycle can also be applied to $VO(acac)_2$ by which it can catalyze the O_2-oxidative polymerization of diphenyl disulfide. Thus the overall redox cycle can be described as Scheme 1. The cycle involves coordination of O_2 to the $[(salen)V^{IV}OV^{III}(salen)]^+$ cation through which oxidation to the $[(salen)V^{IV}OV^{V}O(salen)]^+$ cation takes place. As a result of metal-oxo bond formation ($LM^x + 1/2\ O_2 \rightarrow LM^{x+2}{=}O$), the resulting complex contains two-electron oxidized vanadium(V) and a fully reduced oxo ligand. It is likely that the oxygenation process is promoted by acid. As a next step, the $VOVO^+$ cation is deoxygenated to produce the high-valent $[(salen)V^{IV}OV^{V}(salen)]^{3+}$ complex which will act as a two-electron oxidant for substrates regenerating the low-valent starting complex $[(salen)V^{IV}OV^{III}(salen)]^+$. The unprecedented reactivity of **II** toward

(21) (a) Dotted curves in Figure 6(b) show the current-potential responses obtained at the rotating ring-disk electrode in the absence of O_2. The collection efficiency of the ring maintained at 0.5 V at the electrode rotation rate of 100 rpm (N = 0.27) was slightly less than the intrinsic value of the electrode (N_0 = 0.38) which was determined in independent experiments with ferrocene, implying that VOV^+ was unstable in acidic media. Nevertheless in the presence of excess O_2 (solid curves), the plateau disk current i_D increased with a significant decrease in the plateau ring current i_{R1} measured at 0.5 V where VOV^+ is oxidized, which confirms that VOV^+ is partially consumed by reaction with O_2 during the time required for its transfer from the disk to the ring electrode. Collection experiments of H_2O_2 at the ring electrode maintained at 1.4 V (i_{R2}) were also performed, which revealed that the vanadium complex resulted in a catalysis that causes most of the O_2 to be reduced by four-electrons. The ratio of the ring to disk currents (i_{R2}/i_D) in Figure 6(b), normalized for the perturbed collection efficiency of the ring under O_2 (i_{R1}/i_D), corresponds to the reduction of more than 90% of the O_2 molecules to H_2O. (b) Haberland, D.; Landsberg, R. *Z Electrochem.* **1966**, *70*, 724.

(22) Cyclic voltammograms for a solution of **I** containing aqueous H_2O_2 in acidic CH_2Cl_2 under argon atmosphere showed no catalytic current for the reduction of H_2O_2.

(23) The produced H_2O was detected by ^{1}H-NMR ($CDCl_3$, δ = 1.5 ppm) as follows. The electrolyte solution as in Figure 6 was subject to controlled potential reduction at 0.1 V with a carbon felt electrode to allow catalytic electroreduction of O_2. As a pretreatment for NMR measurement, the resulting solution was oxidized at 0.7 V to diminish the paramagnetic vanadium(IV) species. Analysis for H_2O in the resulting solution was performed by NMR with $CDCl_3$ as a solvent, which revealed that a reasonable amount of H_2O was formed.

O_2 and deoxygenation of **III** and **IV** by protons are suggested as being a key to the performance of these complexes as catalyst for reduction of O_2 to H_2O. The catalytic cycle involves one-step two-electron transfer ($[(salen)V^{IV}OV^{V}(salen)]^{3+} + 2e^- \rightleftarrows [(salen)V^{IV}OV^{III}(salen)]^+$) which would also have essential roles on the catalysis. It may safely be stated that the transfer of multiple isoenergetic electrons is advantageous in the redox reaction: the two-electron oxidation of diphenyl disulfide produces phenyl sulfenyl cation as an active species of the oxidative polymerization. It is a unique model of a catalyst operating in the four-electron reduction of O_2 to H_2O in acidic organic media.

Acknowledgment. We thank Prof. Fred Anson of Caltech for helpful discussions. We also thank Dr. M. Shiro of Rigaku Corporation for his competent assistance in crystallography. This work was partially supported by the Grant-in-Aid for Scientific Research (Nos. 07215282, 07651006, and 08875188) and International Scientific Research Program (Joint Research No. 08044174) from the Ministry of Education, Science, Sports and Culture, Japan.

Supporting Information Available: Tables giving atomic coordinates, equivalent isotropic thermal parameters, and anisotropic displacement parameters for **III** and **IV** (12 pages). See any current masthead page for ordering and Internet access instructions.

JA9617799